Article

Discovery Medicine 2024; 36(188): 1869–1879
https://doi.org/10.24976/Discov.Med.202436188.173

Association of Microbleeds on Susceptibility-Weighted Imaging with Ferroptosis and Prognosis in Rabbits with Spinal Cord Injury

Xing-zhen Liu[1,†], Bo-cheng Wang[2,†], Kang-ping Shen[1], Wen-jie Jin[1,*,§], Jie Zhao[1,*,§]

[1]Department of Orthopaedic Surgery, Shanghai Ninth People's Hospital, Shanghai Jiao Tong University School of Medicine, 200011 Shanghai, China
[2]Department of Radiography, Shanghai Ninth People's Hospital, Shanghai Jiao Tong University School of Medicine, 200011 Shanghai, China
*Correspondence: surgeonjin@126.com (Wen-jie Jin); Profzhaojie@126.com (Jie Zhao)
[†]These authors contributed equally.
[§]These authors contributed equally.
Published: 20 September 2024

Background: Susceptibility-weighted imaging (SWI) is a common imaging technique used to identify cerebral microbleeds. Given that spinal cord injury (SCI) often creates an environment that favors ferroptosis, a type of cell death driven by iron, this study aimed to explore the relationship between microbleeds on SWI and ferroptosis, and explore the effect of deferoxamine on SCI.
Methods: Thirty-six rabbits were divided into three groups: sham, SCI, and SCI with deferoxamine (DFO, a ferroptosis inhibitor) treatment (SCI+DFO). Following 48 hours of SCI modeling, the rabbits underwent magnetic resonance imaging (MRI) and SWI examinations. Ferroptosis markers and spinal cord tissue morphology were examined, and the modified Tarlov's score was used to assess neurological function.
Results: SWI analysis revealed that rabbits in the SCI group exhibited lower signal intensities and larger microbleed areas compared to the those in the SCI+DFO group ($p < 0.05$). The SCI+DFO group demonstrated significantly decreased iron and malondialdehyde (MDA) levels, coupled with increased glutathione (GSH) and glutathione peroxidase 4 (GPX4) levels, along with attenuated ferroptosis ($p < 0.05$). This group also displayed greater Neuronal Nuclei (NeuN) expression, Tarlov's scores, and neurological recovery rates (all $p < 0.05$). A significant positive correlation was found between the microbleed area and iron content (r = 0.59, $p = 0.04$), MDA (r = 0.75, $p = 0.01$), and mitochondrial damage (r = 0.90, $p < 0.01$). Conversely, a negative correlation was established between the microbleed area and GPX4 levels (r = –0.87, $p < 0.01$), as well as neurological function recovery (r = –0.62, $p = 0.03$).
Conclusion: The extent of microbleeds on SWI following SCI is closely correlated with ferroptosis, and the inhibition of ferroptosis could improve neurologic function. These findings suggest that the area of microbleeds on SWI could potentially serve as a predictive marker for ferroptosis in spinal cord injury.

Keywords: sensitivity weighted imaging; microbleeds; spinal cord injury; ferroptosis; prognosis

Introduction

Magnetic resonance imaging (MRI) is regarded as the gold standard for evaluating acute spinal cord injury (SCI), especially for cervical SCI [1]. However, susceptibility-weighted imaging (SWI) has proven to be superior to conventional MRI in detecting hemorrhages associated with SCI [2]. SWI's increased sensitivity to blood degradation byproducts, including deoxyhemoglobin and hemosiderin, renders it a valuable tool for identifying intracerebral microbleeds. However, despite its heightened sensitivity to subtle variations, including local magnetic susceptibility changes and decreased signal-to-noise ratios [3], studies on the SWI sequence for spinal applications are limited. It has been noted that post-hemorrhage, hemoglobin degradation results in the production of heme, a toxic substance implicated in red blood cell death and ferroptosis [4].

Ferroptosis is recognized as a unique type of programmed cell death [5]. The pathological aftermath of SCI sets the stage for ferroptosis. Following SCI, erythrocyte fragmentation and hemolysis occur, releasing substantial amounts of free iron and consequently inducing local iron overload. This provokes stress responses, triggering the activation and subsequent accumulation of numerous lipid-reactive oxygen species [6]. The accumulation of reactive oxygen species is further exacerbated by iron overload. Iron accumulation, lipid peroxidation, glutathione depletion, and glutathione peroxidase 4 (GPX4) depletion have been recognized as crucial regulatory elements of ferroptosis [7]. Therefore, it is plausible to propose a link between SWI-detected microbleeds and ferroptosis in the context of SCI.

Deferoxamine (DFO) has been recognized as a ferroptosis inhibitor [5,6]. DFO has demonstrated the ability to aid in recovery from traumatic SCI by impeding ferroptosis [8], and its efficacy as a treatment modality for SCI has been substantiated [9]. Additionally, in cases of brain injury, DFO has been shown to facilitate the restoration of neural function [10]. This study aimed to explore the relationship between SWI-detected microbleeds and ferroptosis in a rabbit SCI model.

Materials and Methods

Animals

Thirty-six male New Zealand white rabbits, aged between 5 and 6 months, were obtained from Shanghai Jiesijie Experimental Animal Co., Ltd. in Shanghai, China (license number SCXK [Hu] 2018-0004). These rabbits were housed individually in flat-deck cages, adhering to a schedule consisting of 16 h of light and 8 h of darkness. They were housed at room temperature and had free access to water and pellets. The rabbits were randomly and evenly distributed into three groups: a sham group, an SCI group (SCI with saline treatment), and an SCI+DFO group (SCI with DFO treatment). Beginning on the day of surgery and continuing through postoperative day 7, rabbits in the SCI+DFO group received intraperitoneal DFO injections at a dosage of 100 mg/kg (Y0001937 Merck, Darmstadt, Germany) every 12 hours [11]. The SCI group received intraperitoneal injections of 2 mL of 0.9% saline solution at the same intervals. The rabbits underwent intravenous anesthesia using 5% tiletamine hydrochloride and zolazepam hydrochloride (Zoletil50, 8 mg/kg, Virbac, Carros, French) along with 0.05% dexmedetomidine hydrochloride (dexdomitor, 0.01 mg/kg, Zoetis, Shanghai, China). Allen's striking method was employed to induce SCI in rabbits, targeting the T10 with a striking energy of 8 cm × 15 g. This resulted in observable involuntary spastic movements in the lower limbs and twisting of the tail, confirming the successful induction of SCI. In the sham group, laminectomy was performed to expose the dural sac at the T10 segment without inflicting any damage to the spinal cord. After the removal of spinal cord tissue, the rabbits were euthanized with an overdose of sodium pentobarbital (Intravenous, 100 mg/kg). All animal experimental procedures in this study were approved by the Laboratory Animal Ethics Committee at Ninth People's Hospital affiliated with the Shanghai Jiao Tong University School of Medicine, China (SH9H-2022-A94-1).

MRI and SWI Examination

Using a 3.0 T MRI scanner from General Electric (GE Medical Systems Inc, Boston, MA, USA), rabbits were imaged 48 hours post-SCI induction. SWI phase images were scrutinized to identify the largest microbleeds within the T10 spinal cord segments of both SCI and SCI+DFO groups, emphasizing signal intensity, area, and the number of microbleeds. Signal intensity data for the T10 segment were also collected for the sham group. Data were collected in a blinded manner by two independent researchers. MRI parameters included a sagittal T1 weighted imaging (T1WI) with TR 590 ms and TE 40 ms, and a sagittal Dixon sequence T2 weighted imaging (T2WI) with TR 2800 ms, TE 102 ms, a slice thickness of 2.0 mm, slice spacing of 0.5 mm, FOV 160 mm × 160 mm, and matrix 384 × 192. SWI scans were conducted using a 3D Fast Small Angle Gradient Echo Sequence (SWAN) with the following parameters: TR 70 ms, TE 40 ms, slice thickness 2 mm, no gaps, FOV 110 mm × 110 mm, single excitation, 62.50 Hz bandwidth, and a flip angle of 15°, covering from the first thoracic vertebra to the fourth lumbar vertebra. Regions of interest (ROI) were manually drawn on the SWI phase map using the 3.0T GE MRI software (AW Volume Share 5, GE Medical Systems Inc., Boston, MA, USA). For the sham group, the ROI was the central region of the T10 spinal cord, with an area of 3 square mm, and its signal intensity was measured. In the SCI and DFO groups, ROIs were selected from the low-signal area on the SWI phase map corresponding to the T10 spinal cord segment, and the intensity, quantity, and area of the low signal were recorded. Two observers independently reviewed the imaging data, and the average values were calculated for analysis.

Modified Tarlov's Scores

Following the induction of SCI, the modified Tarlov's score was used to evaluate neurological function at several time points: 6 hours, 24 hours, 48 hours, 1 week, 2 weeks, 4 weeks, 6 weeks, and 8 weeks post-injury. At the 8-week mark, spinal cord tissue from the T10 segment was harvested from the rabbits, fixed using 4% paraformaldehyde, and subsequently processed into paraffin-embedded sections for further histological examination.

Hematoxylin and Eosin (HE) Staining

Paraffin sections of rabbit spinal cord tissue were prepared, with subsequent removal of paraffin to facilitate hematoxylin and eosin (HE) staining. The stained sections were then observed under an optical microscope (E100, Nikon, Tokyo, Japan) to examine pathological alterations.

Immunohistochemistry

Eight weeks post-injury, immunohistochemistry was performed on sections of rabbit spinal cord tissue to assess the changes in Neuronal Nuclei (NeuN) and Glial fibrillary acidic protein (GFAP) expression. The tissues were dewaxed and rehydrated, followed by antigen retrieval and blocking with 3% BSA. Next, the tissues were incubated with primary antibodies against NeuN (1:100, DF6145, Affinity, Changzhou, China) and GFAP (1:200, 14-9892-82, Invitrogen, CA, USA) overnight at 4 °C. The next day, HRP-conjugated secondary antibodies (1:200, GB23303,

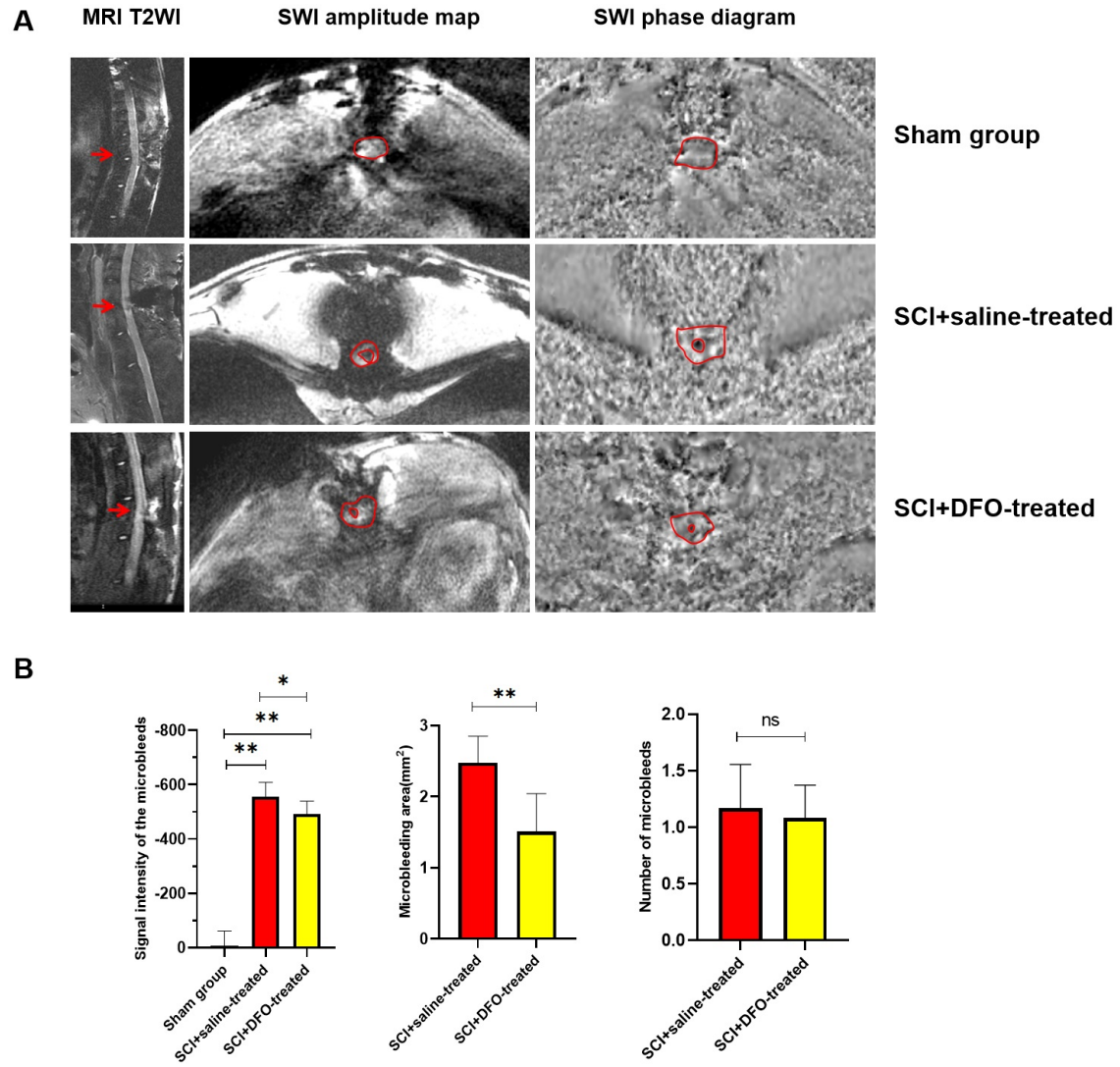

Fig. 1. MRI and SWI changes in the T10 spinal segment of three groups of rabbits 48 hours postoperatively. (A) In the sham group, the SWI signal distribution of rabbit spinal cord tissue was uniform within the red circle, without any low signal shadow. In the SCI and SCI+DFO groups, a low signal shadow was observed in the center of the spinal cord tissue (within the small red circle). Red arrows represent rabbit thoracic segment 10 spinal cord. (B) Changes in signal intensity, microbleed area, and microbleed number were observed in the rabbit spinal cord tissue on SWI (*, $p < 0.05$; **, $p < 0.01$; ns, non-significant, n = 12). MRI, magnetic resonance imaging; SWI, susceptibility-weighted imaging; SCI, spinal cord injury; DFO, deferoxamine; SCI+DFO, SCI with DFO treatment.

Servicebio, Wuhan, China) were applied and incubated for 1 hour at room temperature. Following washes with PBS (pH 7.4), the sections were treated with DAB (GB1211, Servicebio, Wuhan, China) solution to induce color development. Following dehydration and mounting, the sections were examined under a microscope (E100, Tokyo, Nikon, Japan).

Nissl Staining

Paraffin-embedded spinal cord tissue sections underwent dewaxing followed by immersion in Nissl staining solution. These sections were placed in a 60 °C incubator for 50 minutes to facilitate the staining process. Following incubation, the sections were washed thrice with distilled water, and a color separation solution was applied for 1.0 to 2.0 minutes. The sections were then sealed with neutral gum to preserve the staining integrity. Finally, the prepared sections were examined under an optical microscope (E100, Nikon, Tokyo, Japan).

Electron Microscopy

Rabbit spinal cord tissue was preserved, followed by dehydration using a series of ethanol and acetone washes. Subsequently, the tissue underwent infiltration with an acetone/812 embedding resin and was left to polymerize at 60 °C for 48 hours. Ultrathin sections measuring 80 nm

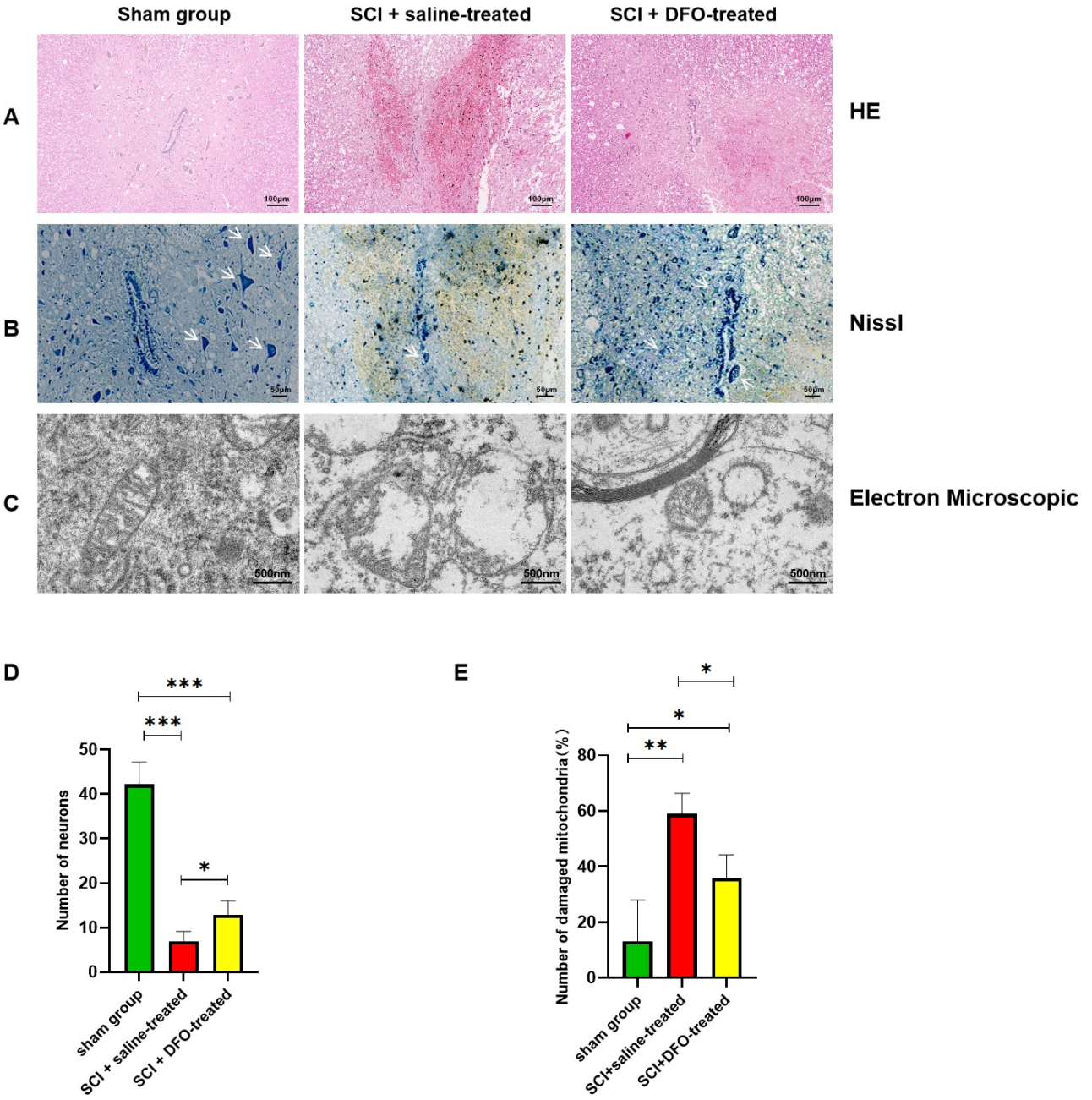

Fig. 2. The effect of ferroptosis inhibitor DFO on rabbit spinal cord tissue 7 days after injury. (A) Hematoxylin-eosin staining. (B) Nissl staining (white arrows represent neurons). (C) Electron microscopy. (D) Changes in the number of neurons in all three groups. (E) The number of damaged mitochondria in all three groups. HE, hematoxylin and eosin. (*, $p < 0.05$; **, $p < 0.01$; ***, $p < 0.001$, n = 6)

were prepared and subsequently stained with a 2% uranium acetate-saturated alcohol solution and lead citrate to enhance contrast. Imaging of these sections was conducted using a transmission electron microscope (model HT7800, Hitachi, Tokyo, Japan).

Western Blot

Spinal cord tissue was retrieved from –80 °C storage for analysis. T10 spinal cord tissue was lysed with a lysis buffer (G2002, Servicebio, Wuhan, China) to extract total protein. Following SDS-PAGE, proteins were transferred onto a PVDF membrane (IPVH00011, Millipore, Billerica, MA, USA) and blocked with 5% non-fat milk at room temperature for 1 hour. The primary antibody GPX4 (67763-1, Proteintech, Wuhan, China) was diluted in TBS buffer (G0001-2L, Servicebio, Wuhan, China) at a dilution ratio of 1:1000 and incubated overnight at 4 °C. The next day, the membrane was incubated for 30 minutes with the secondary antibody (GB23303, Servicebio, Wuhan, China). Protein bands were visualized using an enhanced chemi-

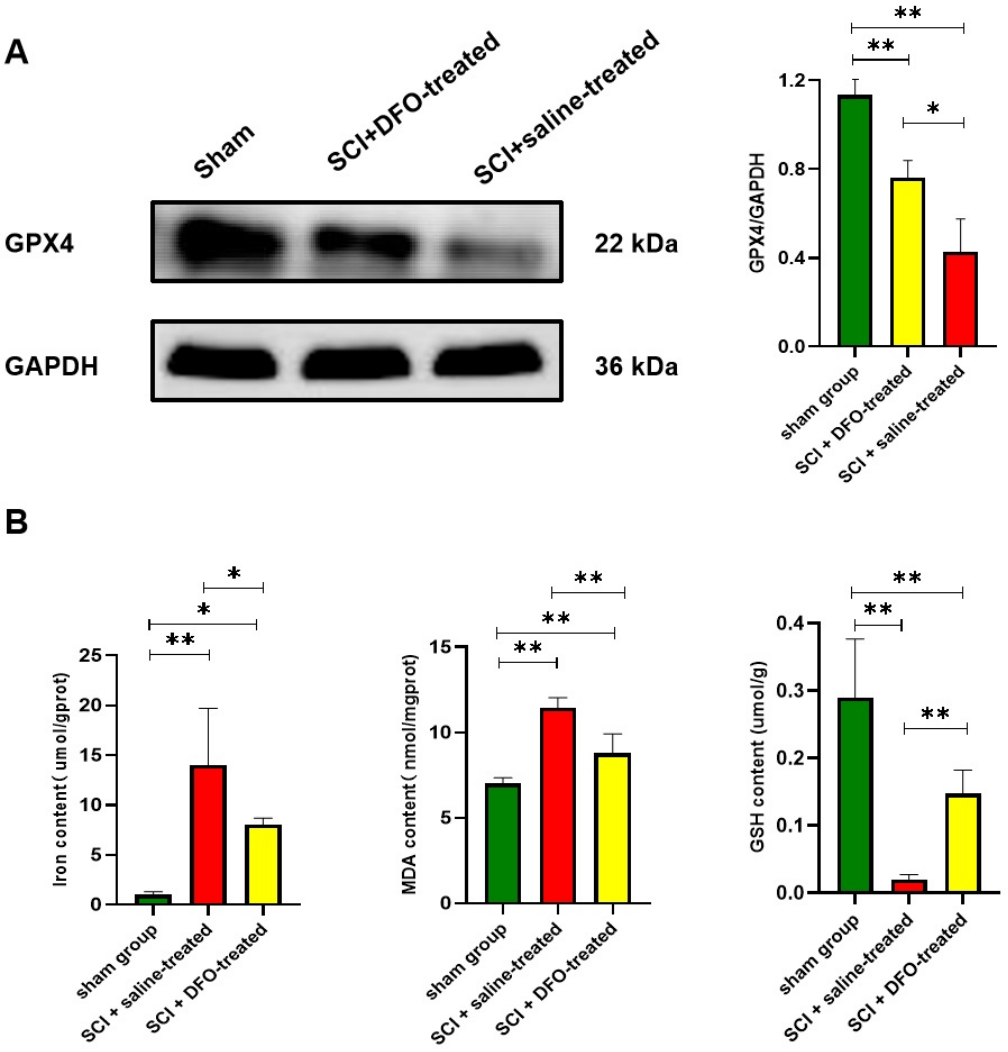

Fig. 3. Changes of GPX4, iron ions, MDA, and GSH in rabbit spinal cord tissue 7 days after spinal cord injury. (A) Changes in GPX4 content in spinal cord tissue (*, $p < 0.05$; **, $p < 0.01$, n = 6). (B) Alterations in iron content, MDA content, and GSH content in rabbit spinal cord tissue (*, $p < 0.05$; **, $p < 0.01$, n = 5). GPX4, glutathione peroxidase 4; MDA, malondialdehyde; GSH, glutathione; GAPDH, glyceraldehyde-3-phosphate dehydrogenase.

luminescence (ECL) detection system (G2014, Servicebio, Wuhan, China), and band scanning was performed. Optical densities (ODs) of the target bands were measured using grayscale analysis software (Alpha EaseFC 4.0, Alpha Innotech, San Leandro, CA, USA). Quantitative analysis was measured using the OD values of the glyceraldehyde-3-phosphate dehydrogenase (GAPDH) bands as a reference for relative expression levels.

Enzyme-Linked Immunosorbent Assay (ELISA)

The content of malondialdehyde (MDA, A003-1), iron ions (A039-2), and glutathione (GSH, A061-2-1) was measured by Enzyme-Linked Immunosorbent Assay (ELISA) according to the manufacturer's instructions provided with the assay kits (Jiancheng Biotechnology Research Institute Co., Ltd., Nanjing, China).

Statistical Analysis

Statistical analysis was conducted using GraphPad Prism software (version 8.0, GraphPad, San Diego, CA, USA). All the data were expressed as mean ± standard error of the mean (SEM). Statistical comparisons between two groups were conducted using a *t*-test, whereas comparisons among three groups were assessed through one-way Analysis of Variance. Pearson's correlation analysis was applied to assess the relationship between two variables. A *p*-value of less than 0.05 was considered statistically significant. Data that did not fit the normal distribution were applied to the Wilcoxon test.

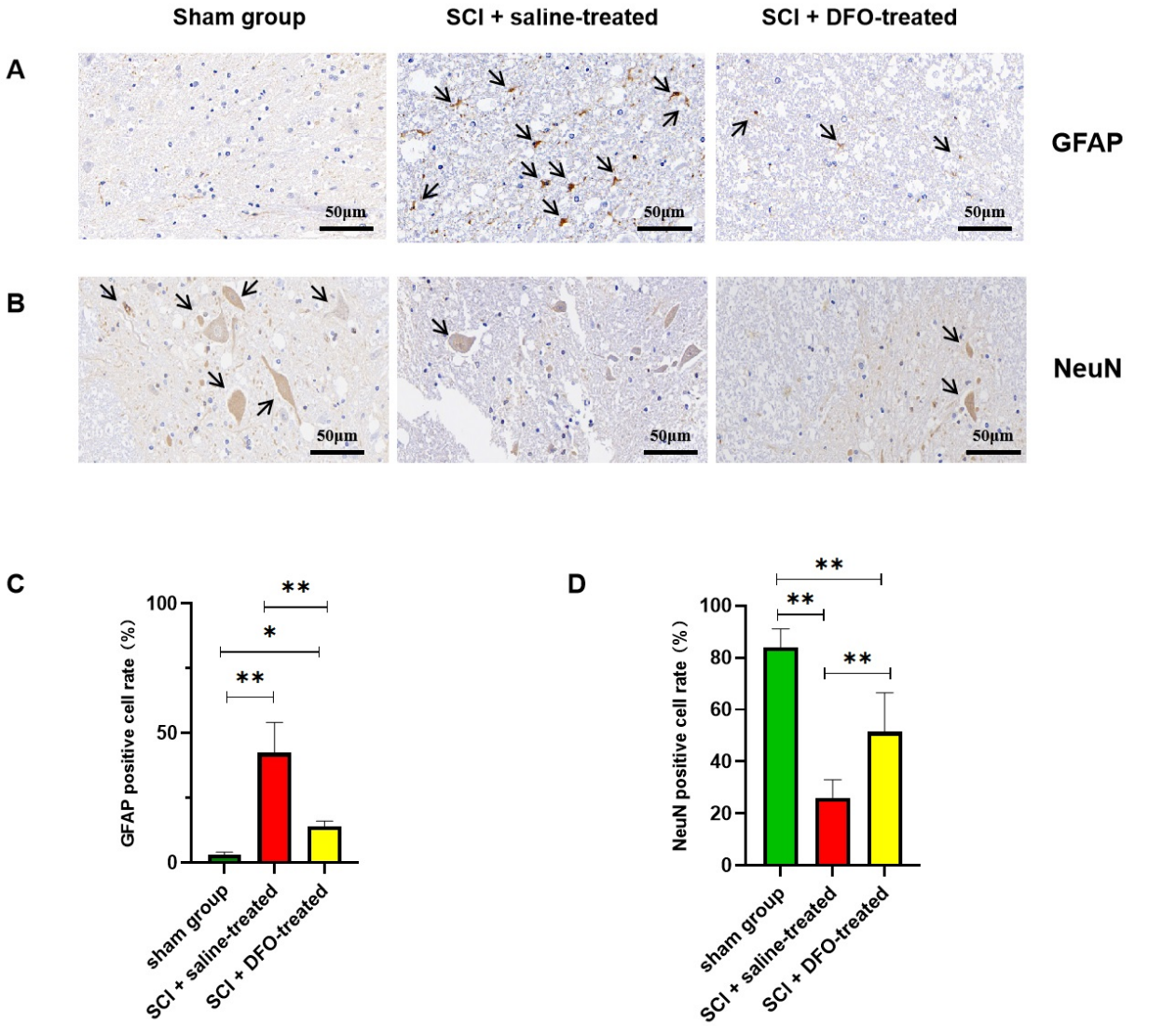

Fig. 4. Changes in neurological function in three groups of rabbits. (A,B) Immunohistochemical examination of GFAP and NeuN in rabbit spinal cord tissue (8 weeks post-surgery). Black arrows represent immunohistochemically positive cells. (C,D) Comparison of the number of GFAP and NeuN positive cells in the three groups of rabbit spinal cord tissue (*, $p < 0.05$; **, $p < 0.01$, n = 6). GFAP, Glial fibrillary acidic protein; NeuN, Neuronal Nuclei.

Results

Microbleed Area was Significantly Higher in the SCI Rabbits

In the sham group, MRI T2WI exhibited normal morphology with a uniform signal, whereas the SCI and SCI+DFO groups demonstrated irregular spinal cord signals. On SWI, both the SCI and SCI+DFO groups presented low signal shadows at the center of the spinal cord tissue. The signal intensity of the spinal cord tissue in the sham group was significantly higher than the SCI and SCI+DFO groups, with the SCI+DFO group displaying a significantly higher signal intensity than the SCI group (all $p < 0.05$). The microbleed area in the SCI group was significantly larger when compared to the SCI+DFO group ($p < 0.01$). Moreover, the number of SWI-detected microbleeds was similar between the SCI and SCI+DFO groups ($p > 0.05$) (Fig. 1A,B).

DFO Ameliorated Histology

In HE staining, the spinal cord tissue of the sham group displayed uniform distribution and normal morphology without signs of bleeding, while the SCI group showed sparsity with visible cavities and patchy bleeding. The SCI+DFO group demonstrated slightly sparse tissue with minor bleeding patches (Fig. 2A). Nissl staining revealed varying neuron counts among the groups: the sham group displayed the highest count, followed by the SCI+DFO group, while the SCI group exhibited the lowest count ($p < 0.05$) (Fig. 2B,D). Electron microscopy analysis revealed

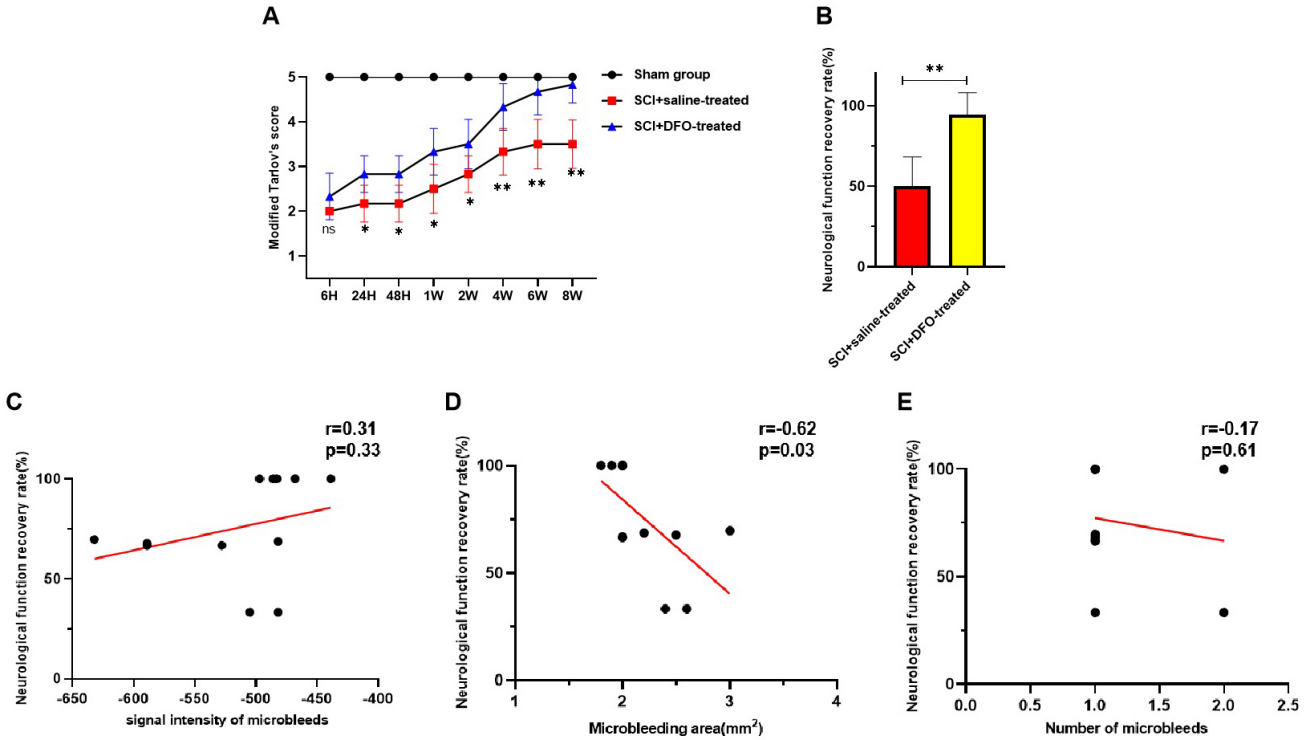

Fig. 5. Changes in neural function and their correlation with microbleeds in three groups of rabbits at 8 weeks post-surgery. (A) Changes in modified Tarlov's scores at various time points after 8 weeks post-surgery in rabbits (*, $p < 0.05$; **, $p < 0.01$; ns, non-significant, n = 6). (B) Neurological recovery rate of rabbits with spinal cord injury at 8 weeks post-surgery (**, $p < 0.01$, n = 6). (C–E) Correlation between microbleed signal intensity, area, and quantity with the neurological recovery rate.

heightened mitochondrial bilayer membrane density and ridge loss in the SCI group. In comparison, the SCI+DFO group exhibited a milder mitochondrial effect. Damaged mitochondria counts were highest in the SCI group, followed by the SCI+DFO group, and lowest in the sham group ($p < 0.05$) (Fig. 2C,E).

DFO Enhanced GPX4 Expression and Inhibited Ferroptosis

The SCI group demonstrated a significant reduction in GPX4 expression compared to both the SCI+DFO and sham groups, with the SCI+DFO group also displaying lower expression relative to the sham group ($p < 0.05$) (Fig. 3A). Regarding iron content, the SCI group demonstrated the highest levels, followed by the SCI+DFO group, while the sham group exhibited the lowest levels ($p < 0.05$). Among the groups, the SCI group displayed the greatest MDA content, indicating oxidative stress ($p < 0.01$). Additionally, GSH content was substantially higher in the SCI+DFO group compared to the SCI group ($p < 0.01$) (Fig. 3B).

DFO Improved Neurological Function

In spinal cord tissue, GFAP-positive cells predominately exhibited yellow staining in the cytoplasm; NeuN-positive cells showed yellow staining in both the nucleus and cytoplasm.

The SCI group exhibited a significantly higher GFAP positivity rate compared to the SCI+DFO group ($p < 0.01$). Additionally, the NeuN positivity rate was significantly lower in the SCI group compared to the SCI+DFO group, with the sham group demonstrating the highest rate ($p < 0.01$) (Fig. 4). At 6 hours post-SCI modeling, the modified Tarlov's scores for both the SCI and SCI+DFO groups were significantly reduced compared to the sham group ($p < 0.05$). However, no significant difference was found between the SCI and SCI+DFO groups ($p > 0.05$). At subsequent time intervals including 24 hours, 48 hours, 1 week, 2 weeks, 4 weeks, 6 weeks, and 8 weeks, the modified Tarlov's scores for the SCI group remained consistently lower than those of the SCI+DFO group ($p < 0.05$). By the 8-week mark, the SCI+DFO group exhibited higher rates of neurological function recovery compared to the SCI group ($p < 0.01$) (Fig. 5A,B).

SWI Intracerebral Microbleeds were Correlated with Neurological Function and Key Indicators of Ferroptosis

No significant correlation was observed between microbleed signal intensity or quantity and the rate of neurological function recovery (all $p > 0.05$). Conversely, a negative correlation existed between the area of microbleeds and the recovery rate (r = –0.62, $p = 0.03$) (Fig. 5C–E). Fur-

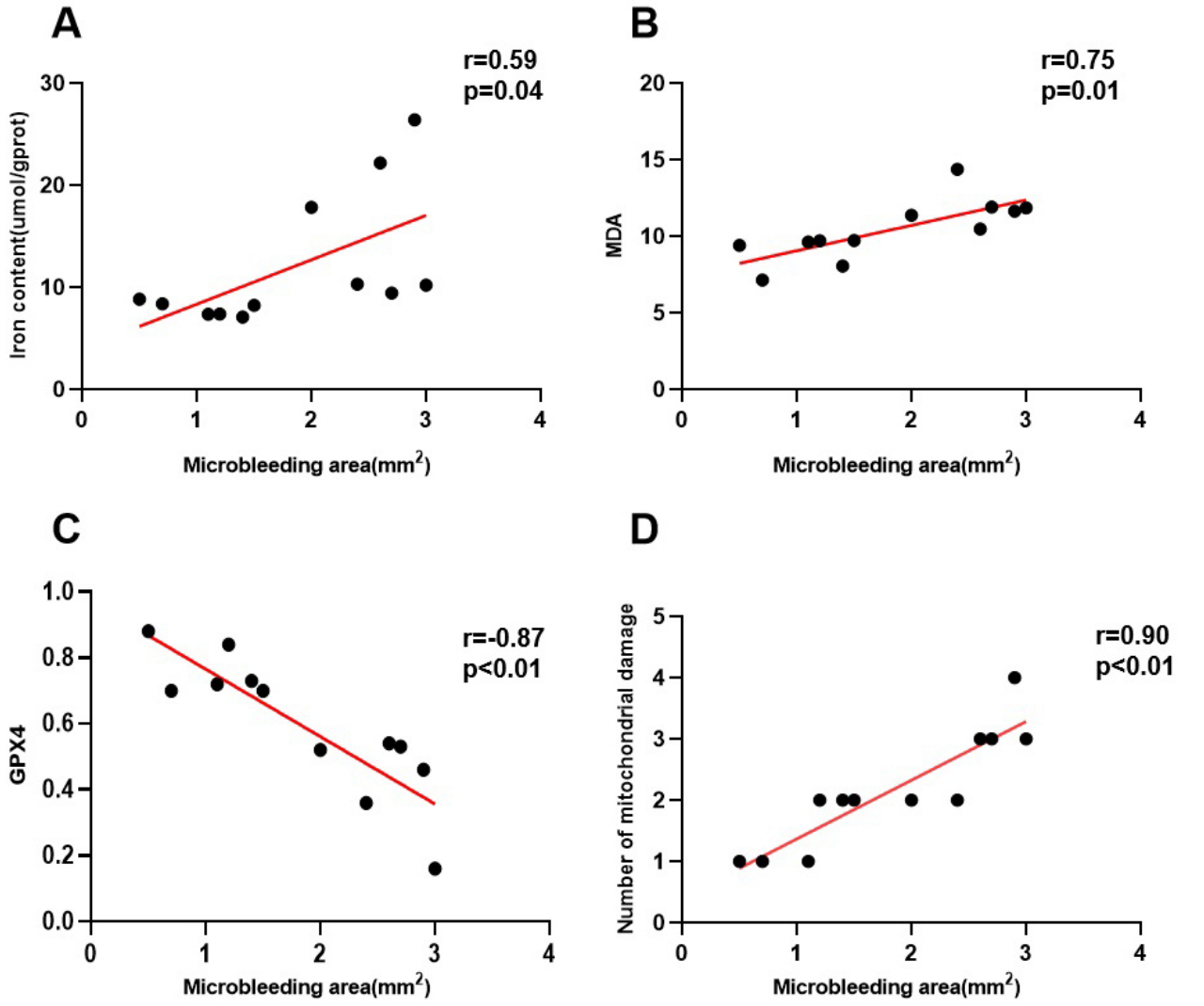

Fig. 6. Correlation between intramedullary microbleeds and ferroptosis in rabbit spinal cord injury. (A) Positively correlated with iron ions. (B) Positively correlated with MDA. (C) Negatively correlated with GPX4. (D) Positively correlated with the number of mitochondrial injuries. (n = 12)

thermore, microbleed area in both the SCI and SCI+DFO groups positively correlated with the content of iron ions (r = 0.59, p = 0.04), MDA levels (r = 0.75, p = 0.01), and the number of damaged mitochondria (r = 0.90, $p <$ 0.01). There was also a negative correlation between the area of microbleeds and GPX4 content (r = –0.87, $p < 0.01$) (Fig. 6).

Discussion

In this study, we observed elevated iron levels in both the SCI and SCI+DFO groups compared to the sham group. Treatment with DFO resulted in decreased iron levels in the SCI+DFO group relative to the SCI group. Although iron ions are essential for bodily functions, an excess can exert neurotoxic effects, including cell death [12,13]. A hallmark of ferroptosis is intracellular iron accumulation. Following SCI, the release of free iron ions from ruptured red blood cells leads to local iron overload. Iron overload can lead to the occurrence of the Fenton reaction, thereby generating reactive oxygen species, promoting ferroptosis [14,15]. The central nervous system naturally exhibits higher iron concentrations compared to other tissues [16,17]. After SCI, there is a significant increase in total iron levels, and SCI-induced hemorrhage results in an influx of red blood cells into the spinal cord, providing an abundance of iron that may exacerbate the situation [18].

GPX4 has been identified as a key regulatory factor for ferroptosis. The inactivation or deletion of GPX4 can lead to the accumulation of lipid peroxides, a lethal characteristic of ferroptosis. The cysteine/glutathione (GSH)/GPX4 axis has been considered central in controlling ferroptosis [19]. Moreover, GSH is known to protect cells from reactive oxygen species (ROS) damage [20]. Given the high levels of polyunsaturated fatty acids in the spinal cord, it is particularly susceptible to peroxidation, which contributes

to secondary damage in SCI [21]. Previous studies have reported a significant reduction in GSH content in post-SCI injury sites [22,23]. In this study, GPX4 and GSH were lower in both the SCI and SCI+DFO groups compared to the sham group, whereas MDA levels were elevated in comparison to the sham group. Research has revealed that the neuroprotective effects of DFO stem from its ability to inhibit ferroptosis, leading to a decrease in iron levels and an increase in GPX4 and GSH [8]. Liu *et al.* [24] reported that DFO reduces iron concentration and lipid peroxidation in SCI rats, thereby enhancing motor function post-injury. Similarly, Dinc *et al.* [25] found that DFO decreases MDA content and facilitates behavioral recovery post-SCI. Consistent with these findings, this study demonstrated that DFO administration increased GPX4 and GSH levels compared to the SCI group. Conversely, the SCI group exhibited increased levels of iron ions and MDA, with a concurrent decrease in GPX4 and GSH. After the introduction of DFO, the SCI+DFO group exhibited reduced levels of iron ions and MDA relative to the SCI group, alongside higher levels of GPX4 and GSH. These observations suggest a potential association between neural dysfunction observed after SCI-related microbleeds and ferroptosis.

SWI demonstrates high sensitivity to paramagnetic substances such as deoxyhemoglobin, oxyhemoglobin, and hemosiderin, commonly found in blood. When tissue bleeding occurs, escaped red blood cells are engulfed by macrophages and degraded by lysosomes. Fe^{3+} ions released from hemoglobin can then bind with proteins and aggregate. When observed under a light microscope, these aggregates appear as large refractive particles with a brownish-yellow color, known as hemosiderin [26]. SWI can detect minuscule hemorrhagic lesions with a diameter smaller than 1 mm, surpassing the detection rate of conventional MRI sequences by at least 67% [27]. Research indicates that bleeding is more prominent in the early stages of acute spinal cord injury, particularly in the gray matter [28]. Moreover, SWI serves as a valuable tool for quantitatively assessing iron deposition, for a technique applicable to organs like the kidneys [29]. Considering the potential of increased iron levels to trigger ferroptosis following spinal cord hemorrhage, SWI emerges as a promising modality for investigating the relationship between iron deposition and ferroptosis. In this study, the SCI group exhibited a larger area of SWI-detected microbleeds and higher iron content compared to the SCI+DFO group. The positive correlation observed between the area of SWI microbleeds and iron ion concentration suggests an association between SWI microbleed area and the extent of ferroptosis. Furthermore, positive correlations with MDA levels and negative correlations with GPX4 substantiate the link between SWI microbleeds and ferroptosis. Thus, a greater SWI microbleed area may indicate more severe ferroptosis.

NeuN stands out as a widely acknowledged marker for mature neurons, known for its sensitivity, stability, and reliability [30]. Conversely, GFAP, highly specific to astrocytes within the central nervous system [31], serves as a marker for complete astrocyte differentiation. In this study, rabbits in the SCI+DFO group demonstrated higher modified Tarlov's scores and NeuN counts, alongside lower GFAP expression compared to the SCI group, indicating superior recovery of neurological functions in the SCI+DFO group. Previous research has demonstrated that patients with microbleeds present with more severe symptoms at 12 months after traumatic brain injury compared to those without microbleeds [32]. This study corroborates these findings, revealing a negative correlation between the area of SWI-detected microbleeds and the rate of neural function recovery in rabbits with SCI. DFO administration resulted in a reduction in the area of SWI-detected microbleeds in the spinal cord and attenuated manifestations of ferroptosis in the SCI+DFO group, thereby yielding a more favorable prognosis for neural function compared to the SCI group. Study has demonstrated that zinc exerts a positive effect on functional nervous system recovery by inhibiting ferroptosis through activation of the nuclear factor E2 pathway [33]. Proanthocyanidins and the ferroptosis inhibitor upregulate the expression and function of GSH and GPX4 post-SCI, thereby enhancing neuronal resistance to membrane phospholipid peroxidation and inhibiting ferroptosis. Consequently, these interventions promote the recovery of motor function post-SCI [34,35]. The predictive capability of the SWI microbleed area on the neural function recovery rate is proposed to be linked to ferroptosis.

The limitations of the article are as follows: Firstly, this study did not utilize SWI in clinical research for spinal cord injury. To enhance the reliability and clinical relevance of SWI in detecting microbleeds after spinal cord injury, future prospective clinical studies should be designed to investigate the application of SWI in microbleed detection post-SCI and its correlation with injury severity (American Spinal Injury Association score). Secondly, there is a lack of specific biomarkers for ferroptosis. This study primarily tests its main phenotype to determine its relationship with SWI microbleeds-related indicators. If specific biomarkers for ferroptosis existed, especially those that can persist over the long term, it would be more beneficial for studying the functional prognosis of spinal cord injury, and the experimental results would be more accurate.

Conclusion

In conclusion, the area of microbleeds demonstrates a close association with ferroptosis in the spinal cord, and DFO could alleviate ferroptosis and improve neurological function. These findings emphasize the potential importance of evaluating microbleed areas in clinical assessments and prognostic considerations for patients with spinal cord injuries.

Availability of Data and Materials

The datasets used and/or analyzed during the current study are available from the corresponding authors on reasonable request.

Author Contributions

JZ and WJ designed this study. XL, BW and KS performed experiments and analyzed experimental data. XL and WJ were responsible for writing this paper. All authors have been involved in revising the manuscript critically for important intellectual content. All authors have given final approval for the version to be published. All authors have agreed to be accountable for all aspects of the work in ensuring that questions related to the accuracy or integrity of any part of the work are appropriately investigated and resolved.

Ethics Approval and Consent to Participate

This study was approved by the Laboratory Animal Ethics Committee in Shanghai Ninth People's Hospital, Shanghai Jiao Tong University School of Medicine, China (Approval number: SH9H-2022-A94-1).

Acknowledgment

Not applicable.

Funding

This study was supported by the National Natural Science Foundation of China, No. 82071564.

Conflict of Interest

The authors declare no conflict of interest.

References

[1] Tarawneh AM, D'Aquino D, Hilis A, Eisa A, Quraishi NA. Can MRI findings predict the outcome of cervical spinal cord Injury? a systematic review. European Spine Journal. 2020; 29: 2457–2464.

[2] Wang M, Dai Y, Han Y, Haacke EM, Dai J, Shi D. Susceptibility weighted imaging in detecting hemorrhage in acute cervical spinal cord injury. Magnetic Resonance Imaging. 2011; 29: 365–373.

[3] Vargas MI, Delattre BMA, Boto J, Gariani J, Dhouib A, Fitsiori A, *et al*. Advanced magnetic resonance imaging (MRI) techniques of the spine and spinal cord in children and adults. Insights into Imaging. 2018; 9: 549–557.

[4] Derry PJ, Vo ATT, Gnanansekaran A, Mitra J, Liopo AV, Hegde ML, *et al*. The Chemical Basis of Intracerebral Hemorrhage and Cell Toxicity With Contributions From Eryptosis and Ferroptosis. Frontiers in Cellular Neuroscience. 2020; 14: 603043.

[5] Dixon SJ, Lemberg KM, Lamprecht MR, Skouta R, Zaitsev EM, Gleason CE, *et al*. Ferroptosis: an iron-dependent form of non-apoptotic cell death. Cell. 2012; 149: 1060–1072.

[6] Xiao W, Yu A, Liu D, Shen J, Xu Z. Ligustilide treatment promotes functional recovery in a rat model of spinal cord injury via preventing ROS production. International Journal of Clinical and Experimental Pathology. 2015; 8: 12005–12013.

[7] Zhang H, Ostrowski R, Jiang D, Zhao Q, Liang Y, Che X, *et al*. Hepcidin Promoted Ferroptosis through Iron Metabolism which Is Associated with DMT1 Signaling Activation in Early Brain Injury following Subarachnoid Hemorrhage. Oxidative Medicine and Cellular Longevity. 2021; 2021: 9800794.

[8] Yao X, Zhang Y, Hao J, Duan HQ, Zhao CX, Sun C, *et al*. Deferoxamine promotes recovery of traumatic spinal cord injury by inhibiting ferroptosis. Neural Regeneration Research. 2019; 14: 532–541.

[9] Shi J, Tang R, Zhou Y, Xian J, Zuo C, Wang L, *et al*. Attenuation of White Matter Damage Following Deferoxamine Treatment in Rats After Spinal Cord Injury. World Neurosurgery. 2020; 137: e9–e17.

[10] Wan J, Ren H, Wang J. Iron toxicity, lipid peroxidation and ferroptosis after intracerebral haemorrhage. Stroke and Vascular Neurology. 2019; 4: 93–95.

[11] Ren S, Han S, Wang L, Huang Y, Wu J, Wu G. Minimally Invasive Surgery for ICH Evacuation Combined With Deferoxamine Treatment Increased Perihematomal Claudin-5 and ZO-1 Expression Levels and Decreased BBB Permeability in Rabbits. Frontiers in Neurology. 2022; 13: 835494.

[12] Schwartz G, Fehlings MG. Secondary injury mechanisms of spinal cord trauma: a novel therapeutic approach for the management of secondary pathophysiology with the sodium channel blocker riluzole. Progress in Brain Research. 2002; 137: 177–190.

[13] Chen Z, Gao C, Hua Y, Keep RF, Muraszko K, Xi G. Role of iron in brain injury after intraventricular hemorrhage. Stroke. 2011; 42: 465–470.

[14] Tang D, Chen X, Kang R, Kroemer G. Ferroptosis: molecular mechanisms and health implications. Cell Research. 2021; 31: 107–125.

[15] Chen X, Yu C, Kang R, Tang D. Iron Metabolism in Ferroptosis. Frontiers in Cell and Developmental Biology. 2020; 8: 590226.

[16] Mehta JR, Braund KG, Toivio-Kinnucan M. Elemental composition, water, and total lipid content in peripheral nerves, spinal cord and brain of healthy adult dogs. Research in Veterinary Science. 1990; 49: 250–252.

[17] Zaleska MM, Floyd RA. Regional lipid peroxidation in rat brain in vitro: possible role of endogenous iron. Neurochemical Research. 1985; 10: 397–410.

[18] Koszyca B, Manavis J, Cornish RJ, Blumbergs PC. Patterns of immunocytochemical staining for ferritin and transferrin in the human spinal cord following traumatic injury. Journal of Clinical Neuroscience. 2002; 9: 298–301.

[19] Lei P, Bai T, Sun Y. Mechanisms of Ferroptosis and Relations With Regulated Cell Death: A Review. Frontiers in Physiology. 2019; 10: 139.

[20] Toyokuni S, Ito F, Yamashita K, Okazaki Y, Akatsuka S. Iron and thiol redox signaling in cancer: An exquisite balance to escape ferroptosis. Free Radical Biology & Medicine. 2017; 108: 610–626.

[21] Imai H, Matsuoka M, Kumagai T, Sakamoto T, Koumura T. Lipid Peroxidation-Dependent Cell Death Regulated by GPx4 and Ferroptosis. Current Topics in Microbiology and Immunology. 2017; 403: 143–170.

[22] Zhou KL, Chen DH, Jin HM, Wu K, Wang XY, Xu HZ, *et al*. Effects of calcitriol on experimental spinal cord injury in rats. Spinal Cord. 2016; 54: 510–516.

[23] Du F, Wang X, Shang B, Fang J, Xi Y, Li A, *et al*. Gastrodin ameliorates spinal cord injury via antioxidant and anti-inflammatory effects. Acta Biochimica Polonica. 2016; 63: 589–593.

[24] Liu J, Tang T, Yang H. Protective effect of deferoxamine on experimental spinal cord injury in rat. Injury. 2011; 42: 742–745.
[25] Dinc C, Iplikcioglu AC, Atabey C, Eroglu A, Topuz K, Ipcioglu O, *et al*. Comparison of deferoxamine and methylprednisolone: protective effect of pharmacological agents on lipid peroxidation in spinal cord injury in rats. Spine. 2013; 38: E1649–E1655.
[26] Rouault TA. Iron metabolism in the CNS: implications for neurodegenerative diseases. Nature Reviews. Neuroscience. 2013; 14: 551–564.
[27] Nandigam RNK, Viswanathan A, Delgado P, Skehan ME, Smith EE, Rosand J, *et al*. MR imaging detection of cerebral microbleeds: effect of susceptibility-weighted imaging, section thickness, and field strength. AJNR. American Journal of Neuroradiology. 2009; 30: 338–343.
[28] Sekhon LH, Fehlings MG. Epidemiology, demographics, and pathophysiology of acute spinal cord injury. Spine. 2001; 26: S2–S12.
[29] Sun J, Sha Y, Geng W, Chen J, Xing W. Susceptibility-weighted Imaging for Renal Iron Overload Assessment: A Pilot Study. Magnetic Resonance in Medical Sciences. 2022; 21: 415–424.
[30] Sarnat HB, Nochlin D, Born DE. Neuronal nuclear antigen (NeuN): a marker of neuronal maturation in early human fetal nervous system. Brain & Development. 1998; 20: 88–94.
[31] Zhang Z, Zoltewicz JS, Mondello S, Newsom KJ, Yang Z, Yang B, *et al*. Human traumatic brain injury induces autoantibody response against glial fibrillary acidic protein and its breakdown products. PLoS ONE. 2014; 9: e92698.
[32] Hageman G, Hof J, Nihom J. Susceptibility-Weighted MRI and Microbleeds in Mild Traumatic Brain Injury: Prediction of Post-traumatic Complaints? European Neurology. 2022; 85: 177–185.
[33] Ge MH, Tian H, Mao L, Li DY, Lin JQ, Hu HS, *et al*. Zinc attenuates ferroptosis and promotes functional recovery in contusion spinal cord injury by activating Nrf2/GPX4 defense pathway. CNS Neuroscience & Therapeutics. 2021; 27: 1023–1040.
[34] Zhou H, Yin C, Zhang Z, Tang H, Shen W, Zha X, *et al*. Proanthocyanidin promotes functional recovery of spinal cord injury via inhibiting ferroptosis. Journal of Chemical Neuroanatomy. 2020; 107: 101807.
[35] Zhang Y, Sun C, Zhao C, Hao J, Zhang Y, Fan B, *et al*. Ferroptosis inhibitor SRS 16-86 attenuates ferroptosis and promotes functional recovery in contusion spinal cord injury. Brain Research. 2019; 1706: 48–57.